NEOPLASIA
www.neoplasia.com
Volume 35 Number xxx Month 2023 pp. 100853

Original Research/Original Research Article

Lipolysis-stimulated lipoprotein receptor-targeted antibody-drug conjugate demonstrates potent antitumor activity against epithelial ovarian cancer☆,☆☆

Mizuki Kanda[a,b,c]; Satoshi Serada[b,*]; Kosuke Hiramatsu[a]; Masashi Funauchi[a,b,c]; Kengo Obata[d]; Satoshi Nakagawa[a]; Tomoharu Ohkawara[c]; Okinori Murata[c]; Minoru Fujimoto[c]; Fumiko Chiwaki[e]; Hiroki Sasaki[e]; Yutaka Ueda[a]; Tadashi Kimura[a]; Tetsuji Naka[c,**]

[a] Department of Obstetrics and Gynecology, Osaka University Graduate School of Medicine, Osaka, Japan
[b] Institute for Biomedical Sciences Molecular Pathophysiology, Iwate Medical University, Yahaba, Iwate, Japan
[c] Division of Allergy and Rheumatology, Department of Internal Medicine, School of Medicine Iwate Medical University, Yahaba, Iwate, Japan
[d] Division of Oral and Maxillofcial Surgery, Department of Oral and Maxillofacial Reconstructive Surgery, School of Dentistry, Iwate Medical University, Morioka, Iwate, Japan
[e] Department of Translational Oncology, National Cancer Center Research Institute, Tokyo, Japan

Abstract

Background

Epithelial ovarian cancer (EOC) is a lethal malignant tumor, for which new treatment options are urgently required. Lipolysis-stimulated lipoprotein receptor (LSR) is widely expressed in EOC, and it is associated with poor prognosis. In this study, we developed an antibody-drug conjugate (ADC) targeting LSR as a new therapeutic approach to EOC.

Methods

We, herein, developed novel anti-LSR monoclonal antibodies (mAbs) and an LSR-ADC by conjugating monomethyl auristatin E as a payload. We subsequently evaluated the *in vitro* and *in vivo* (on xenograft models) antitumor effect of the LSR-ADC.

Results

An overexpression of LSR was observed not only in the primary EOC tumor but also in its lymph node and omental metastases. The EOC cell lines NOVC7-C and OVCAR3 strongly expressed LSR (as compared to ES2 cells). Both the anti-LSR mAb and the LSR-ADC were able to specifically bind to LSR-positive cells and were rapidly internalized and trafficked to the lysosomes. The LSR-ADC demonstrated a potent antitumor effect against NOVC-7C and OVCAR3, but little activity against ES2 cells. *In vitro*, the LSR-ADC exhibited a potent antitumor effect against NOVC-7C and OVCAR3. Moreover, in the OVCAR3 xenograft models as well as in

Abbreviations: ADC, antibody-drug conjugate; BLI, bioluminescence imaging; mAb, monoclonal antibody; mAbs, monoclonal antibodies; EOC, Epithelial ovarian cancer; IHC, Immunohistochemical; LSR, Lipolysis-stimulated lipoprotein receptor; MMAE, monomethyl auristatin E; PDX, patient-derived xenograft.

* Corresponding author. Satoshi Serada, Institute for Biomedical Sciences Molecular Pathophysiology, Iwate Medical University, 1-1-1 Idaidori, Yahaba-cho, Shiwa-gun, Iwate 028-3694, Japan.

** Co-corresponding author. Tetsuji Naka, Division of Allergy and Rheumatology, Department of Internal Medicine, School of Medicine Iwate Medical University, 2-1-1 Idaidori, Yahaba-cho, Shiwa-gun, Iwate 028-3695, Japan.

E-mail addresses: serada@iwate-med.ac.jp (S. Serada), tnaka@iwate-med.ac.jp (T. Naka).

☆ **Financial support**

☆☆ This research was supported by AMED under Grant Number JP17im0210606 and JP20im0210111.

Received 8 June 2022; received in revised form 5 November 2022; accepted 8 November 2022

https://doi.org/10.1016/j.neo.2022.100853

the patient-derived xenograft models of LSR-positive EOC, the LSR-ADC significantly inhibited tumor growth. The LSR-ADC also suppressed the omental/bowel metastases in OVCAR3-Luc xenografts and improved the median survival.

Conclusion

The developed LSR-ADC demonstrated a significant antitumor activity against LSR-positive EOC cell lines and tumors. Our preclinical data support the use of the LSR-ADC as a novel therapy for patients with LSR-positive ovarian cancer.

Neoplasia (2023) 35, 100853

Keywords: Antibody-drug conjugate, Lipolysis-stimulated lipoprotein receptor, Ovarian cancer

Introduction

Epithelial ovarian cancer (EOC) is one of the most lethal malignant tumors occurring in women: 13,940 and 4,700 EOC-associated deaths have been registered in 2020 in the United States [1] and Japan [2], respectively. Half of the EOC patients are diagnosed at an advanced stage with peritoneal dissemination and lymph node metastases [3]. The standard treatment for EOC consists of cytoreductive surgery and chemotherapy with a combination of platinum compounds and taxanes. Although the EOC initially responds to these agents, it soon acquires chemoresistance, thereby leading to tumor relapse [4–8]. Second-line or later-line therapeutic agents provide a median survival of 9−12 months, with a response rate of approximately 20% for these patients. [4–6], Therefore, new treatment options are required to overcome recurrent and refractory EOC.

Antibody-drug conjugates (ADCs) are antibodies conjugated with cytotoxic drugs *via* a cleavable or a noncleavable linker. Cytotoxic drugs are delivered to the cell that expresses the antigen through monoclonal antibodies (mAbs) and are internalized by the cells. The selectivity of the antibody can reduce the cytotoxicity of normal tissues and the nonspecific consumption of the drug [9,10]. To date, more than 150 ADCs have been assessed in clinical trials [11]; however, the commercially available ADCs for the treatment of EOC are still limited [12]. Notably, we have already demonstrated that the glypican-1-targeted ADC exhibits efficacy against uterine cervical cancer, pancreatic cancer, and esophageal cancer [13–17]. We have also reported that the CD70-ADC shows an antitumor activity against leiomyosarcoma and ovarian cancer. [18,19] We, herein, apply these results to the development of new therapeutic agents for EOC.

We have previously identified the lipolysis-stimulated lipoprotein receptor (LSR) as a new tumor antigen of EOC, by using iTRAQ-based quantitative proteomics [20]. LSR was originally identified in the liver as an oleate-activated receptor [21,22]. Apart from its function as a lipoprotein, its overexpression in different cancer types has been widely reported, with head and neck carcinoma [23], lung cancer [24], colon cancer [25], bladder cancer [26], breast cancer [27], gastric cancer [28], and endometrial cancer [29] being among them. In particular, LSR has been associated with the proliferation and invasion of cancer cells [24]. As previously reported by us, about 70% of serous carcinoma and 50% of clear cell carcinoma patient tissues seem to express LSR. We have also demonstrated that the overall survival of EOC patients with a high LSR expression was significantly shorter than that of patients with a low LSR expression. Thus, LSR is a poor prognostic factor, and it is widely expressed in EOC patient tissues and EOC cell lines, while LSR expression in human normal tissues is very low [20]. Therefore, we thought that LSR could be a good candidate for an antibody-based therapy against EOC. In preclinical efficacy studies, the anti-LSR mAb (#1-25) inhibited the proliferation of LSR-positive tumors by 60%−80% (as compared to control mIgG2a that inhibits lipid uptake). With the expectation of inducing stronger effects, we proceeded in generating a novel anti-LSR antibody that was conjugated with the potent microtubule-disrupting agent monomethyl auristatin E (MMAE). We subsequently assessed the expression of LSR in EOC patients and investigated the possibility of employing the LSR-ADC as a novel therapeutic target.

Material and methods

Cell lines

NOVC-7C cells were kindly gifted by Hiroki Sasaki (National Cancer Center Research Institute, Tokyo, Japan) in 2020: they were established by a patient-derived ascites [30–32]. OVCAR3 cells were obtained from the RIKEN BioResource Research Center, while OVCAR-3/CMV-Luc cells (OVCAR3-Luc) were obtained from the Japanese Collection of Research Bioresources. Finally, the ES2 cells were obtained from the American Type Culture Collection. NOVC7-C, OVCAR3, and OVCAR3-Luc were grown in RPMI 1640 medium (Wako Pure Chemical Industries) with 10% fetal bovine serum (FBS; Serum Source International) along with 100 U/mL penicillin, and 100 μg/mL streptomycin (Nacalai Tesque). ES2 cells were grown in McCoy's 5A medium (Gibco) with 10% FBS, 100 U/mL penicillin, and 100 μg/mL streptomycin. Cells were cultured at 37°C, under a humidified atmosphere of 5% CO_2. All cell lines were confirmed to be mycoplasma-free by using a MycoAlert Mycoplasma Detection Kit (Lonza).

Patients and tissue samples

The formalin-fixed, paraffin-embedded, 4-μm tissue sections of five EOC patients were collected for the undertaking of immunohistochemistry (IHC). Supplementary Table 1 provides a summary of the relevant clinicopathological information. Informed consent was obtained by all patients, and the experimental protocol was approved by the ethics committee of Iwate Medical University (MH2021-057). All patient studies were conducted in accordance with the Declaration of Helsinki.

Preparation of the ADC

We prepared the anti-LSR mAb (#16-6) and the isotype control antibody (mouse IgG2a, clone MOPC-173; BioLegend, San Diego, CA) to synthesize the ADC. The anti-LSR mAb was partially reduced with tris-(2-carboxyethyl-phosphine) hydrochloride, followed by a reaction with maleimidolacaproyl-valine-citrulline-paminobenzyloxycarbonyl-MMAE to yield the LSR-ADC and control-ADC. MMAE belongs to the dolastatin-10 family of highly potent antimitotic agents that inhibit tubulin polymerization; it is often

used as the drug in the construction of an ADC. To remove any residual unreactive toxins, the conjugated ADCs were desalted on Sephadex G50 columns, the buffer was exchanged for phosphate-buffered saline (PBS), and the resulting ADC-containing solution was filtered. The drug distribution was then analyzed by hydrophobic interaction chromatography.

Internalization studies

The internalization assay was conducted according to the procedure described by Austin *et al*. [33] OVCAR3 cells (2×10^5 cells) were stained with an Alexa Fluor 488-labeled anti-LSR mAb (#16-6) (10 μg/mL) for 1 h, at 4°C. After washing, the cells were incubated for internalization as indicated hours, at 37°C. The incubated cells were fixed with 1% paraformaldehyde overnight, at 4°C, in the dark. The fixed cells were washed and treated with an anti-Alexa488 antibody (10 μg/mL) for the quenching of the fluorescence on the cell surface. To detect the signals, the cells were analyzed by a FACS Canto II cytometer. The internalization rate (%) was calculated by using the following equation:

$$\{1 - (N_a - Q_a)/(N_a - N_a \times Q_i/N_i)\} \times 100,$$

where N_a is the mean fluorescence intensity (MFI) of the sample at each incubation time point without quenching, Q_a is the MFI of the sample at each incubation time point with quenching, N_i is MFI of the pre-incubation sample without quenching, and Q_i is MFI of the pre-incubation sample with quenching.

Cytotoxicity assay

Cytotoxicity assays were performed in the presence of the anti-LSR mAb (#16-6), the mouse IgG2a isotype control antibody, the LSR-ADC or the control-ADC. The cytotoxicity of these agents was assessed by using cells growing (at a cell density of 500 to 4,000 cells per well) in a normal growth medium in flat-bottom 96-well white polystyrene plates (Thermo Fischer Scientific). After 24 h, the cells were incubated with serial dilutions of the agents in triplicate wells for 144 h, at 37°C, in a humidified 5% CO_2 atmosphere. Cell viability was determined with the CellTiter-Glo Luminescent Cell Viability Assay Kit (Promega, WI), and luminescence values were measured by using a microplate reader (SPARK). The obtained results are reported as IC_{50}; the concentration of compound needed to yield a 50% reduction in viability, as compared to vehicle-treated cells (control: 100%).

Cell cycle assay

Cells (OVCAR3, NOVC-7C) were prepared in 6-well plates at densities of 2×10^5 cells per well. After 24 h, the tumor cells were supplemented with 16 nM LSR-ADC (MMAE) or control-ADC (MMAE) in quadruplicate wells and were incubated for 24 h, at 37°C, in a humidified 5% CO_2 atmosphere. Cell cycle analysis was performed by using the Cycle Test Plus DNA Reagent kits (BD Biosciences) and the FACS Canto II flow cytometer, as previously described.

Caspase-3/7 activity assay

Cells were prepared in 96-well white polystyrene plates (Thermo Fisher Scientific) at densities of 500−4,000 cells per well, in a normal growth medium. After 24 h, tumor cells were supplemented with serial dilutions of LSR-ADC (MMAE) or control-ADC (MMAE) in triplicate wells, and were incubated for 48 h, at 37°C, in a humidified 5% CO_2 atmosphere. The activities of caspase-3 and -7 in the cell cultures were detected by using Caspase Glo 3/7 Assays (Promega), as previously described.

In vivo *efficacy study in an ovarian cancer cell line and a patient-derived xenograft (PDX) model*

Healthy five- to six-week-old female severe combined immunodeficient (SCID) and non-obese diabetic/Shi-scid-IL2Rγ null (NOG) mice were purchased from Charles River Japan and the Central Institute for Experimental Animals, respectively. For the undertaking of the xenograft experiments, SCID mice were subcutaneously inoculated with OVCAR3 cells at a total volume of 100 μL in 1:1 PBS/Matrigel (Becton Dickinson). The PDX model was generated by implanting small fragments (approximately 10 mm^3) of the surgically resected tumor that had not received any preoperative radiotherapy or chemotherapy into the NOG mice, subcutaneously. These PDX mice were named Ovx6. The use of human tissue was permitted by the ethics committee of the Osaka University Hospital (09011-2).

Tumors were measured twice (OVCAR3 xenograft) or once (Ovx6) a week with the use of vernier calipers. Tumor volumes were calculated by the following formula:

$$\text{tumor volume } \left(mm^3\right) = \text{length} \times \text{width} \times \text{width} \times 0.5.$$

When the average volumes reached 110 mm^3, the mice were divided into four groups, and the treatment was initiated. PBS, varying doses of LSR-ADC (1, 3, or 10 mg/kg), anti-LSR mAb (#16-6) (10 mg/kg) or control antibody (mouse IgG2a, Biolegend, #400281, CA, USA) (10 mg/kg) were intravenously administered in 200 μL of PBS, twice a week, for a total of four times. Tumors were resected 28 days (OVCAR3) or 70 days (Ovx6) after the start of the treatment. All animal experiments were conducted in compliance with the institutional ethical guidelines for animal experimentation of the Iwate Medical University (2-35, MH2021-200).

To further investigate the pharmacological action of LSR-ADC at the cellular level *in vivo*, the population of mitotic cells was measured after the treatment. Animals bearing OVCAR3 tumor xenografts were injected with PBS or LSR-ADC (1, 3, or 10 mg/kg) and the tumors were harvested after 24 h and resected. The IHC analysis was performed with the use of an antibody against a mitotic marker, anti-phospho-Histone H3 (Ser10) (#9701, Cell Signaling Technologies, 1:400), as described in the "IHC: performance and photography" section.

In vivo *efficacy study in an omental/bowel metastasis xenograft model*

OVCAR-3/CMV-Luc cells (1×10^7 cells in 400 μL PBS) were injected intraperitoneally into the subscapular areas of 5–6 week-old female SCID mice [34]. The extent of the omental/bowel metastasis was measured by using the IVIS Lumina Imaging System (Xenogen Corporation, Hopkinton, MA). When the luciferin intensity of the tumors in the mice reached 5×10^5 to 2×10^7 phot/sec, the mice were randomized into two groups, and the treatment was initiated. PBS or LSR-ADC (MMAE; 10 mg/kg) were intravenously administered twice a week, for a total of four times. The tumor burden was measured once a week, by using the IVIS Lumina Imaging System. The body weights and the clinical status of the mice were evaluated twice a week.

Statistical analysis

Data are presented as mean ± SD for the *in vitro* experiments, and as mean ± SEM for the *in vivo* experiments. For the comparisons among three or more groups, the values were analyzed through one-way ANOVA, followed by a Holm-Sidak test. The Kaplan–Meier survival analysis was calculated by the log-rank test. Differences were considered significant at $p < 0.05$.

Other experiments are described in the Supporting Information Methods.

Table 1

IC_{50} values for MMAE, LSR-ADC and control-ADC in ovarian cancer cell lines.

Cell lines	Morphology	LSR expression (ABC/cell)	LSR-ADC (nM)	Control-ADC (nM)	MMAE (nM)
NOVC7C	CCC	84008.8	1.743	N.D.	0.372
OVCAR3	HGSOC	89382.9	0.449	N.D.	0.286
OVCAR3-LUC	HGSOC	86697.7	0.193	N.D.	0.167
ES2	CCC	2631.9	N.D.	N.D.	0.330

Abbreviation: ABC = antibody binding capacity, ADC = antibody-drug conjugate, LSR = lipolysis stimulated lipoprotein, MMAE = monomethyl auristatin E, CCC = clear cell carcinoma, HGSOC = high grade serous ovarian cancer, N.D. = not determined

Results

LSR is highly expressed in primary EOC and metastatic lesions

We evaluated the LSR expression in the primary tumors, lymph node metastases, and omental metastases of five EOC patients through IHC (Figure 1A). LSR was homogenously expressed on the membrane of tumor cells. In the metastatic lesions, the intensity and morphology of the IHC staining were similar to those of the respective primary tumor. Notably, the expression of LSR was much lower in hepatocytes in the normal liver compared to tumor cells (Supplementary Figure 1). Thus, these results indicate that the LSR expression is markedly high in primary EOC and preserved in the metastatic lesions, and the LSR-ADC efficacy in these lesions was anticipated.

LSR is strongly expressed in EOC cell lines

We confirmed the altered expression of LSR in EOC cell lines by flow cytometry. Two human ovarian high-grade serous carcinoma cell lines (OVCAR3, OVCAR3-Luc) and two human ovarian clear cell carcinoma cell lines (NOVC-7C, ES2) were evaluated (Figure 1B). The NOVC-7C, OVCAR3, and OVCAR3-Luc cell lines highly expressed LSR. The expression of LSR was low in ES2 cells (Figure 1B), and we used ES2 cells as a negative control in the following experiments. The quantitative measurement (by flow cytometry) of the LSR expression on the cell membrane revealed similar results; LSR-positive cell lines have higher values (NOVC-7C: 84008.8 sites/cell; OVCAR3: 89382.9 sites/cell; OVCAR3-Luc: 86697.7 sites/cell), whereas ES2 exhibited low values (2631.9 sites/cell; Table 1). Western blotting also showed a higher LSR expression in the NOVC-7C, OVCAR3, and OVCAR3-Luc cell lines (Figure 1C). These results support the notion that the LSR was strongly expressed in ovarian cancer. We utilized these LSR-positive and -negative cell lines in an *in vitro* model.

Selection of an LSR-binding mAb, and production of an LSR-ADC

LSR is overexpressed in various malignant solid cancers, as compared to a low expression in normal tissues. Therefore, we considered LSR to be an attractive candidate for the development of an ADC. Previously, our group developed five clones of the anti-LSR mAb (namely, #1-25, #9-7, #16-6, #26-2, and #27-6) [20]. To identify the optimal mAb for the production of an LSR-targeting ADC, these mAbs were screened, and they were evaluated (through an indirect cytotoxicity assay) by their ability to deliver an auristatin payload into LSR-expressing cells *in vitro*, after exposing cells to anti-LSR mAb and an MMAF-conjugated secondary antibody. Among the five anti-LSR mAbs, clone #16-6 exhibited the lowest IC_{50} (Supplementary Table 2), suggesting that this clone was the most efficient in delivering the MMAF-conjugated secondary antibody into the LSR-positive cells. We, thereby, selected clone #16-6 for the antibody component of the LSR-ADC. The anti-LSR mAb (#16-6) or an isotype control mouse IgG2a were directly conjugated with MMAE. The drug-to-antibody ratio was 2.8 for LSR-ADC, and 3.5 for control-ADC (Figure 2A). We calculated the K_D value of the anti-LSR mAb and the LSR-ADC in OVCAR3 cells, to evaluate the effect of MMAE conjugation on the affinity of the anti-LSR mAb (unconjugated anti-LSR mAb (#16-6): K_D = 1.054 nM, binging max = 2,660; LSR-ADC: K_D = 0.677 nM, binding max = 2,552) (Figure 2B). We were, thereby, convinced that the MMAE conjugation did not inhibit the antibody-binding activity.

Internalization of LSR-ADC was confirmed in OVCAR3 cells

At first, the kinetics of the internalization of the anti-LSR mAb (#16-6) were measured by flow cytometry, after exposure of OVCAR3 cells to an Alexa488-labeled anti-LSR mAb (#16-6). Anti-LSR mAb (#16-6) was efficiently internalized with an average rate of 89.6% at 1 h after binding to the cell surface LSR (Figure 2C). We subsequently visualized the translocation of the anti-LSR mAb (#16-6) and the LSR-ADC to the lysosomes by immunofluorescence (Figure 2D). The anti-LSR mAb (#16-6) and the LSR-ADC bound to the cell membrane when incubated at 4°C, prior to the initiation of the internalization assay. By incubating at 37°C for 2 h, the membrane staining of the LSR was decreased and was instead moved into the lysosomes, as evidenced by the overlap of staining for LSR and the lysosomal marker LAMP-1. These results suggest that the LSR-ADC bound to the membrane of the LSR-expressing cells is internalized and translocated to the lysosomal compartment.

LSR-ADC successfully inhibited the proliferation of OVCAR3 and NOVC-7C cells

To demonstrate that the binding and the internalization of LSR-ADC leads to a selective killing of the LSR-expressing human ECC cell lines, a cell growth assay using anti-LSR antibodies (#16-6), LSR-ADCs, and MMAE were performed with the use of LSR-positive (NOVC-7C and OVCAR3) and LSR-negative cells (ES2). While the unconjugated anti-LSR mAb (#16-6) had no effect on the viability of any of the cell lines, the LSR-ADC caused a dose-dependent decrease in cell viability in both the OVCAR3 and the NOVC-7C cells *in vitro* (Figures 3A and 3B). None of the cell lines treated in this study were found to be drug resistant to MMAE, with an IC_{50} of around 0.3 nM. The IC_{50} values of the LSR-positive cells were 0.19−1.74 nM, and the IC_{50} of the LSR-ADC for the LSR-negative ES2 cells was not calculated since the cell inhibitory rate at 16 nM did not reach 50% (Table 1). The unconjugated anti-LSR mAb (#16-6) exhibited no cytotoxicity at concentrations up to 66.6 μM (data not shown). Additionally, we examined the effect of LSR-ADC (MMAE) on the cell cycle and apoptosis. The LSR-ADC (MMAE) significantly increased the proportion of cells in the G_2/M phase, whereas the control-ADC did not affect it (Figure 3C). This is attributed to the microtubule polymerization arrest caused by MMAE. In addition, the LSR-ADC (MMAE) caused a dose-dependent increase in the caspase-3/7 activity, as compared to that of the control-ADC (MMAE)

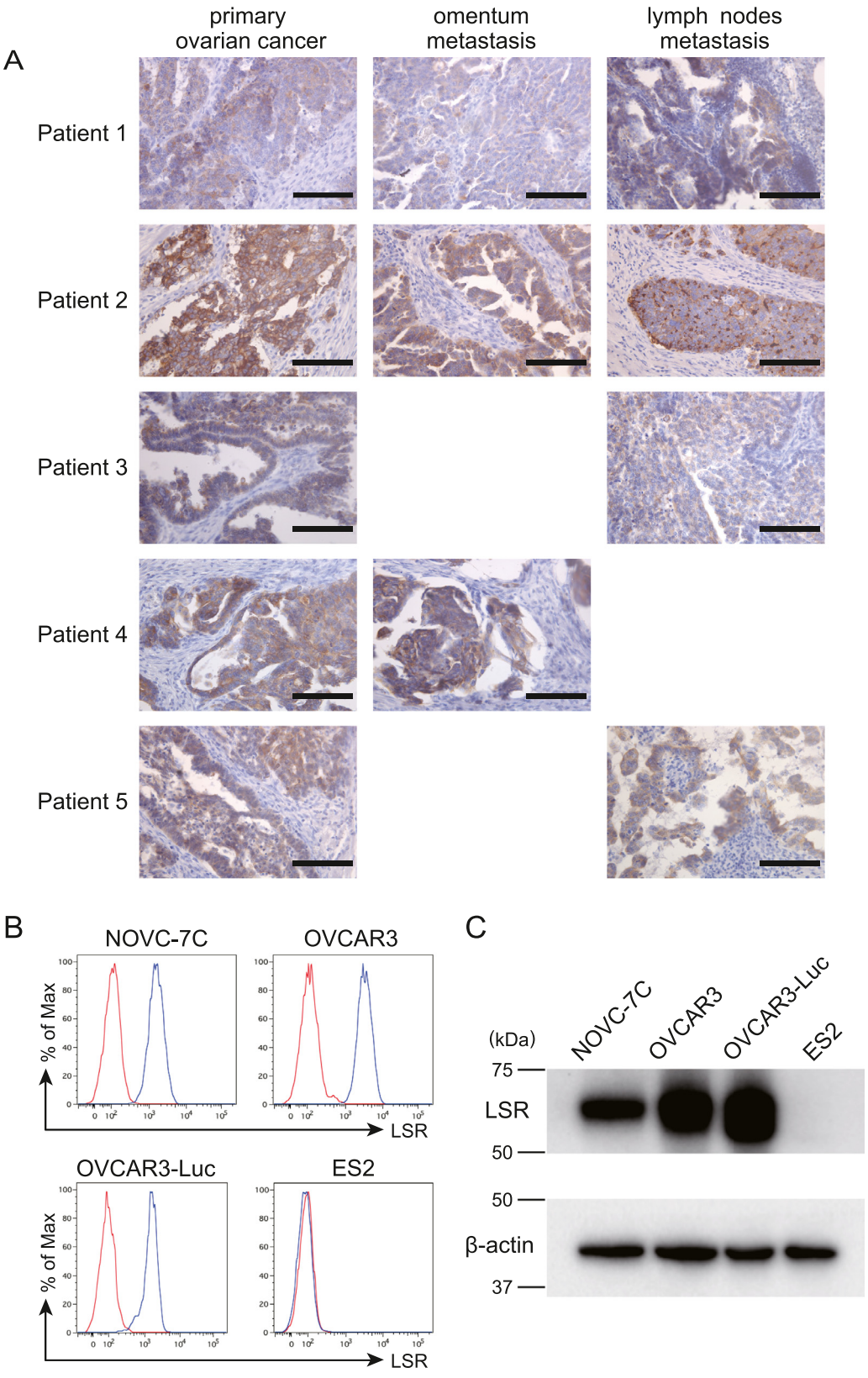

Fig. 1. Analysis of lipolysis-stimulated lipoprotein receptor (LSR) expression in epithelial ovarian cancer (EOC). **(A)** Immunohistochemistry (IHC) was performed for LSR in primary EOC, lymph node metastases, and metastases in the omentum of five patients with EOC. Scale bars: black = 100 μm. **(B)** Flow cytometry of the LSR expression in NOVC-7C, OVCAR3, OVCAR3-Luc, and ES2 cells, as detected with an anti-LSR monoclonal antibody. **(C)** Western blotting analysis of the LSR expression in NOVC-7C, OVCAR3, OVCAR3-Luc, and ES2 cells, as detected with an anti-LSR monoclonal antibody.

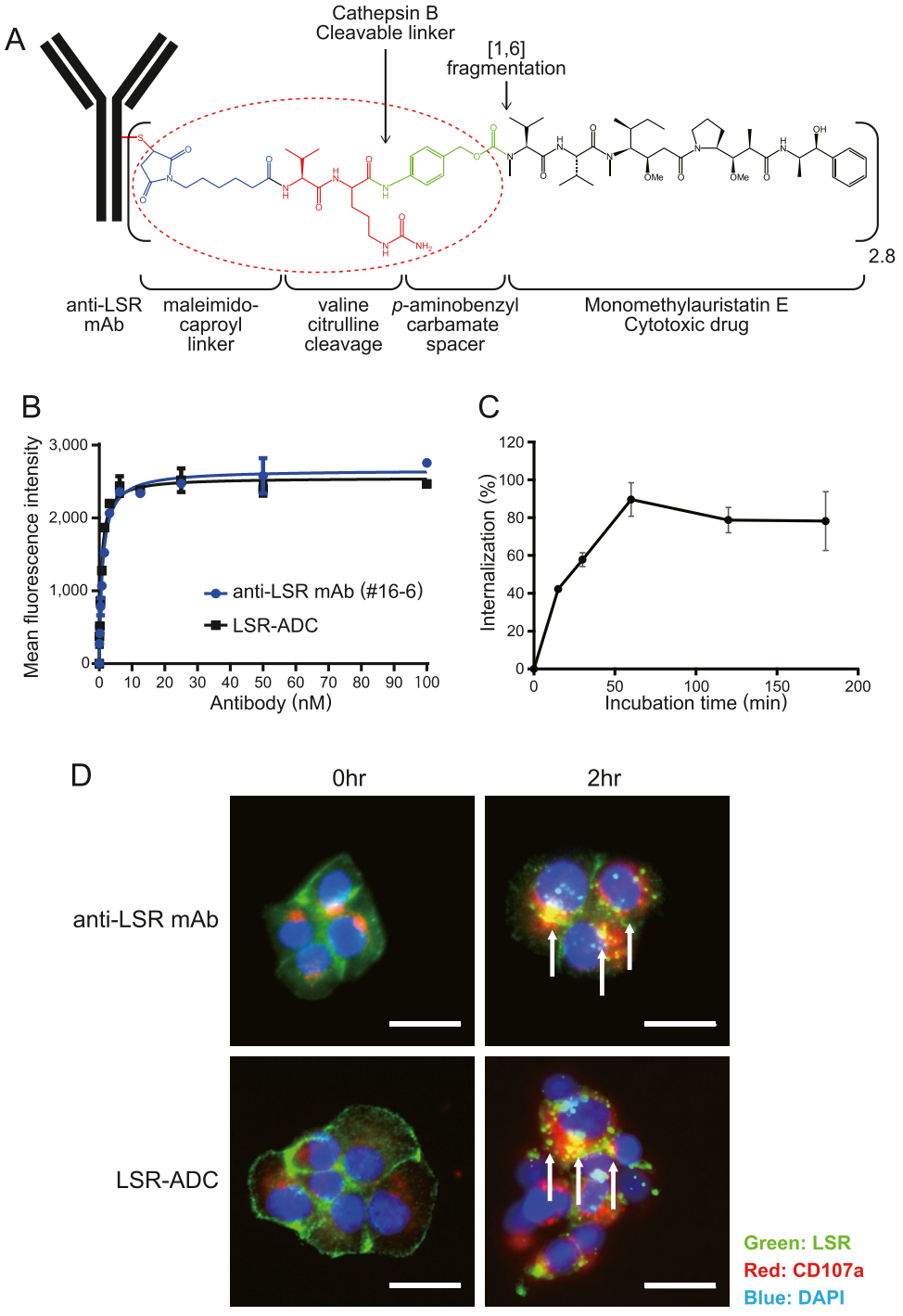

Fig. 2. Structure, binding affinity, and internalization activity of an anti-lipolysis-stimulated lipoprotein receptor monoclonal antibody (anti-LSR mAb; #16-6) and a lipolysis-stimulated lipoprotein receptor antibody-drug conjugate (LSR-ADC). **(A)** The structure of the LSR-ADC consists of the anti-LSR mAb (#16-6) that is conjugated to a monomethyl auristatin E (MMAE) payload. **(B)** OVCAR3 cells were incubated with the unconjugated anti-LSR mAb (#16-6; blue closed circles) or with the LSR-ADC (black closed rectangles). Mean fluorescence intensity at various concentrations is shown. **(C)** Time-course analysis of the internalization activity of anti-LSR mAb (#16-6) in OVCAR3 cells. **(D)** Detection of the internalization activity of anti-LSR mAb (#16-6) or LSR-ADC by fluorescence microscopy in OVCAR3 cells. Cell surface and intracellular LSR are visualized. Green indicates LSR, red indicates the lysosomal marker CD107a, and blue indicates DAPI(4′,6-diamidino-2-phenylindole)-stained DNA. Scale bar: 25 μm.

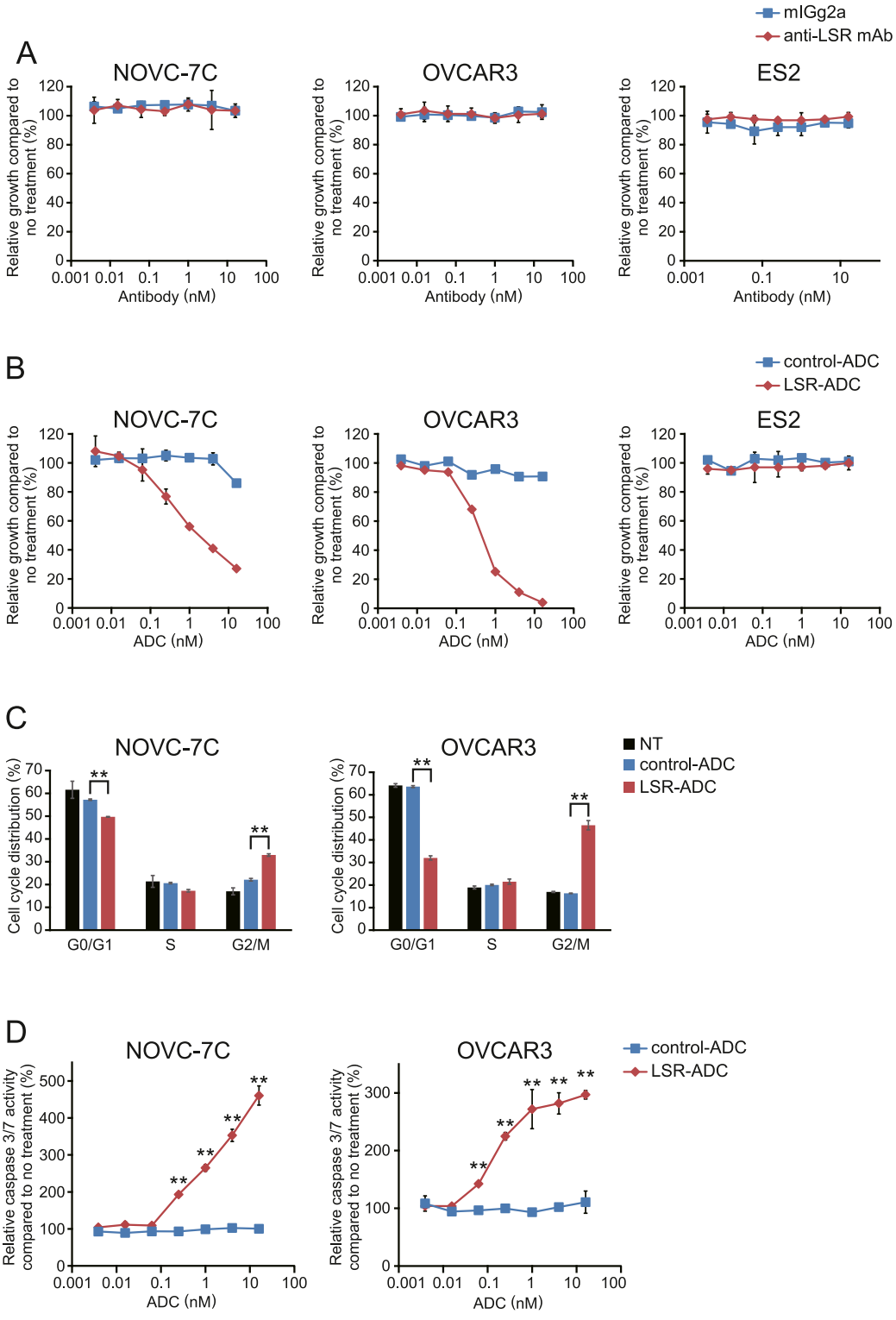

Fig. 3. *In vitro* cell growth inhibitory activity of LSR-ADC. **(A)** NOVC-7C, OVCAR3, and ES2 cells were treated with the anti-LSR mAb (#16-6) or with the control IgG antibody for 144 h. Neither antibody inhibited the cell growth in any of the cell lines. **(B)** The cells were treated with LSR-ADC or with mouse IgG2a-ADC (control-ADC) for 144 h. LSR-ADC significantly inhibited the growth of LSR-positive NOVC-7C and OVCAR3 cell lines (as compared to control-ADC). In the LSR-negative ES2 cell line, neither treatment had any inhibitory effect. **(C)** Induction of G_2/M phase cell cycle arrest in NOVC-7C and OVCAR3 cells treated with LSR-ADC. Cells were treated with either 16 nM control-ADC or 16 nM LSR-ADC. After 24 h, a cell cycle analysis was performed by flow cytometry, with the use of propidium iodide DNA staining. **: $p < 0.01$ (as determined by one-way ANOVA, followed by a Dunnett's *post hoc* test). **(D)** Induction of apoptosis in NOVC-7C and OVCAR3 cells treated with LSR-ADC. Cells were treated with control-ADC or LSR-ADC for 48 h. Caspase-3/7 activity was monitored by using the Caspase Glo 3/7 assay system. The caspase-3/7 activity that was relative to untreated cells was detected in cells treated with increasing concentrations of LSR-ADC. **: $p < 0.01$ (as determined by Student's *t*-test).

(Figure 3D). Thus, the LSR-ADC (MMAE) induced a cell cycle arrest at the G_2/M phase and promoted apoptosis through the caspase-3/7-dependent pathway.

LSR-ADC showed potent tumor growth inhibition in OVCAR3 xenografts and the PDX model

We evaluated the therapeutic effects of LSR-ADC on ovarian cancer *in vivo*, by establishing two kinds of xenograft models. One of these models was established by subcutaneously implanting OVCAR3 cells into CB17/SCID mice and the other model was a PDX named Ovx6, which was generated by implanting human tumor tissues expressing LSR at high levels. IHC revealed that the expression of LSR in the tumor tissues of xenografted mice was high and its pattern was homogenous. When the mean tumor size of each cancer type reached approximately 110 mm^3, PBS or LSR-ADC were intravenously injected twice a week, for a total of four times. The anti-LSR mAb (#16-6) and the control antibody were administered in the same way. In OVCAR3 xenografts, the growth of the tumors treated with 3 mg/kg of LSR-ADC was significantly suppressed (as compared to that of the PBS group) after day 7 ($p < 0.05$). More importantly, after day 7, the treatment with 10 mg/kg of LSR-ADC significantly suppressed the tumor growth even further than the treatment with lower doses did ($p < 0.001$; Figure 4A). The treatment with anti-LSR mAb (#16-6) displayed a weak tumor growth inhibition when compared to the one with LSR-ADC (Supplementary Figure 2). In the Ovx6 model, the treatment with 3 mg/kg of LSR-ADC significantly suppressed the tumor growth (as compared to that of the PBS group) after day 21 ($p < 0.05$). The treatment with 10 mg/kg of LSR-ADC suppressed the tumor growth even further than the treatment with lower doses did after day 21 ($p < 0.001$; Figure 4B). The tumor growth inhibitory effect of LSR-ADC on Ovx6 was more slowly exerted than that on the OVCAR3 xenografts. This is more likely due to differences in the original tumor growth speed, rather than due to differences in the LSR expression since the immunostaining of Ovx6 tumors obtained similar levels of LSR expression to those obtained by the OVCAR3 xenografts. No significant weight loss was observed in any of the treatment groups of mice, in either the case of the OVCAR3 xenografts or that of the Ovx6 model (Figures 4A and 4B).

To further analyze the pharmacological action of LSR-ADC *in vivo*, the population of mitotic cells was measured after treatment. An IHC staining of the phosphorylated histone H3 (Ser10) of the OVCAR3 xenograft tumors was performed (Figure 4C). As expected, a marked increase in the percentage of tumor cells undergoing mitosis was detected after treatment with LSR-ADC, but not with PBS. These results suggest that the tubulin-polymerizing inhibitor MMAE was effectively delivered into the LSR-expressing tumor cells by the anti-LSR mAb, thereby causing mitotic arrest.

LSR-ADC (MMAE) suppresses the omental/bowel metastases in OVCAR3-Luc xenografts

To assess the efficacy of LSR-ADC against omental/bowel metastasis, OVCAR3-Luc xenograft models were used. We established OVCAR3-Luc xenograft models by implanting OVCAR3-Luc cells intraperitoneally, into the subscapular areas. Imaging and weight measurement were performed weekly after the inoculation. The general condition of the mice was monitored three times a week. Six or seven weeks after the inoculation, the luciferase activity of the tumors in the mice reached 5×10^5 to 2×10^7 phot/sec, and the treatment was initiated. PBS and 10 mg/kg of LSR-ADC were intravenously injected twice a week, for a total of four times. LSR-ADC (MMAE) suppressed the elevation of the tumor burden on day 14 and day 21 ($p < 0.05$) (Figures 5A and B). By day 28 (11 weeks after the inoculation), the mice appear to have gained weight ($p < 0.01$; Figure 5C) and have developed clinically appreciable ascites [35]. After the ascites developed, the measurement of the luciferase activity does not seem to recapitulate the tumor growth, as already reported by a previous study [36]. We adopted the Beart's criteria [36] of euthanasia for this ovarian cancer model, and we sacrificed the mice when their respiratory frequency increased or when they showed no spontaneous movement. When compared to the treatment with PBS, the treatment with LSR-ADC (MMAE) significantly improved the median survival of the mice (from 43 to 59 days; $p < 0.01$; Figure 5D).

Discussion

In this study, we demonstrated that LSR was highly expressed on the cell surface of primary EOC and metastatic lesions. We developed a unique LSR-ADC and characterized its antitumor activity. To our knowledge, this is the first study to demonstrate the efficacy of an ADC that targets LSR. The developed LSR-ADC exhibited potent efficacy, both *in vitro* and *in vivo*, when compared to a naked anti-LSR mAb, with limited toxicity. The therapeutic effect of LSR-ADC was observed not only in the local but also in the metastasis model, thereby prolonging the survival of mice.

The efficacy of an ADC is prescribed by several factors, such as the expression levels of the target antigen, the binding affinity of the ADC for the antigen, the efficacy of internalization into the cells, and the cytotoxicity of the drug [37,38]. The utility of the LSR-ADC can be explained from these points. At first, the LSR is widely expressed in ovarian cancer cell lines; as mentioned in the "Introduction," 50%−70% of the ovarian cancer patient specimens have been found to be strongly positive for LSR, and a higher LSR expression has been associated with poor prognosis [20]. The IHC analysis shows that the LSR is stained in a homogenous manner among the tumor cells. In this study, the LSR expression was observed not only in the primary tumor but also in metastatic sites, thereby suggesting that the LSR might be a useful target for antibody-based therapy. Secondarily, the anti-LSR mAb exhibits a high-binding affinity and an internalization efficiency. The K_D values of the anti-LSR mAb and the LSR-ADC were 1.054 nM and 0.677 nM, respectively; the binding affinity of the latter is as high as the typical K_D values for antibodies used in ADCs (nM-range or lower) [39,40]. In addition, the measurement of the internalization kinetics displayed that the anti-LSR mAb (#16-6) was rapidly internalized into the cells after binding to LSR on cancer cells. The internalization speed of the anti-LSR mAbs (#16-6) was comparable to the one of the ADCs already in clinical use [40]. Thirdly, we selected MMAE as the drug to conjugate with the anti-LSR mAb (#16-6) to produce the LSR-ADC. MMAE is a microtubule polymerization inhibitor, which is one of the most frequently chosen payloads for ADCs against gynecologic malignancies [12]. In this study, the MMAE was found to be strongly effective against various ovarian cancer cell lines. This suggests that, as long as the LSR is expressed, the LSR-ADC will have a potent antitumor effect. As MMAE only interferes with the microtubule dynamic dividing cells, our ADC would be expected to exert only moderate toxicity, since normal cells are characterized by lower LSR expression levels and lower rates of cell division. For these reasons, we present LSR-ADC as a novel therapeutic strategy for LSR-positive EOC cases; it is a compound that exerts high affinity, high internalizing rates, and a potent anti-cancer activity.

Administration of the naked anti-LSR mAb (#16-6) led to a slight tumor growth inhibition (as compared to control IgG against subcutaneous OVCAR3 xenograft mice; Supplementary Figure 2), which is weaker than that of the anti-LSR mAb (#1-25) [20]. Tumor growth inhibition by anti-LSR mAbs could be owing to the inhibition of lipid uptake (as previously described in EOC xenograft models [20]) or to an immune response (such as the antibody-dependent cellular cytotoxicity or the complement-dependent cytotoxicity). The anti-LSR mAb (#16-6) seems to have a lower tumor inhibition ability, but it is characterized by a higher internalization ability. The conjugation of MMAE to the anti-LSR mAb (#16-6) leads to a stronger antitumor effect, than that of the naked anti-LSR mAb (#16-6).

There are several limitations to this study. Firstly, there is a need to explore the threshold of the LSR expression levels at which the LSR-ADC

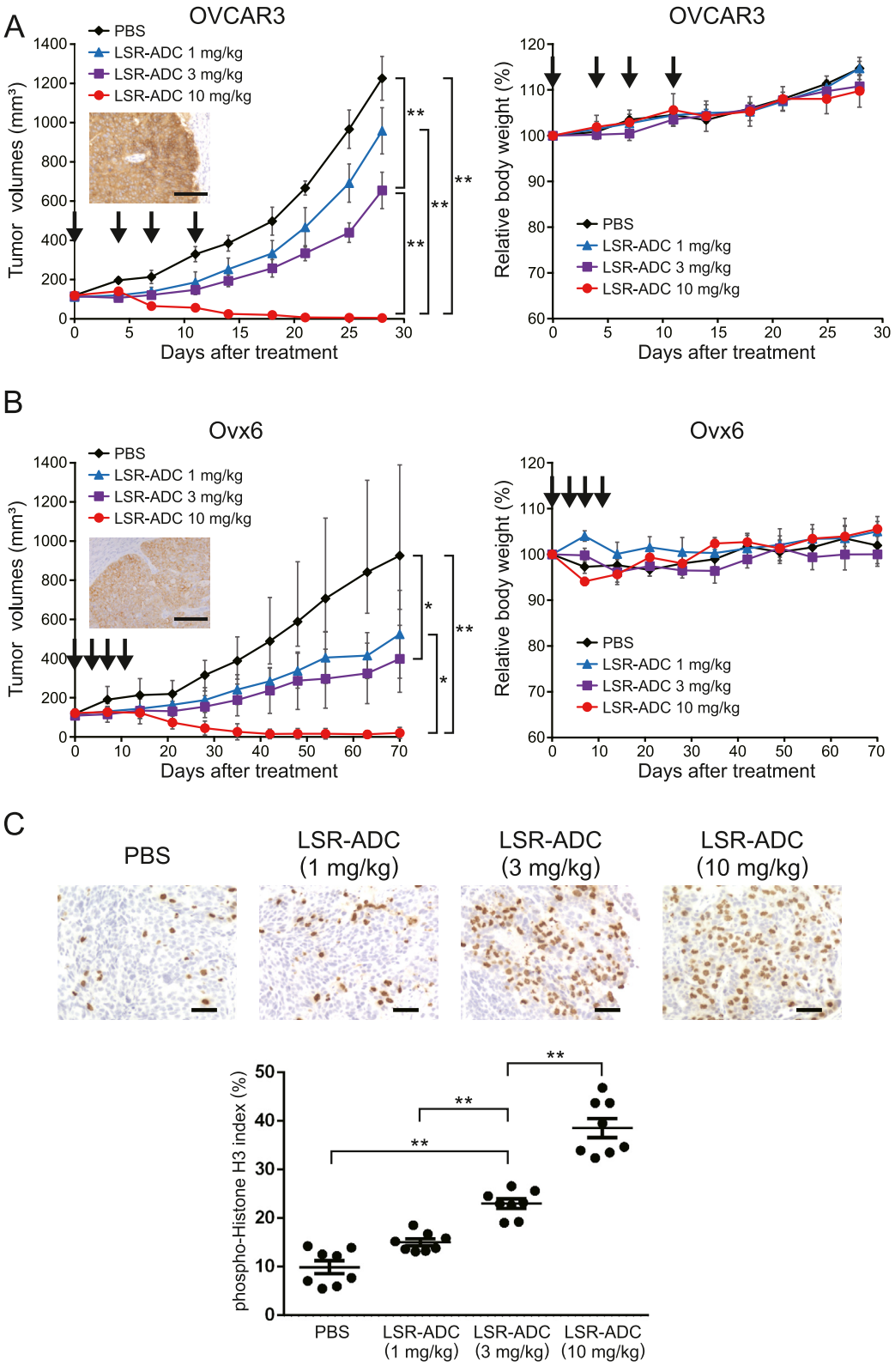

Fig. 4. *In vivo* antitumor activity of LSR-ADC. **(A, B)** Antitumor efficacy of LSR-ADC in OVCAR3 xenografts (n = 6/group) and PDX, Ovx6 (n = 6/group) models. Tumor volumes are presented in the left panel. Representative images of IHC staining for LSR in xenografted tumor tissues from untreated mice are inserted. Scale bar: 100 μm. The tumor-bearing mice were given phosphate-buffered saline (PBS) or LSR-ADC (1, 3, or 10 mg/kg) intravenously, twice a week, for a total of four times. Each point on the graph represents the average tumor volume. Changes in body weight are also presented in the right panel. Black arrows indicate the timing of the PBS or the LSR-ADC administration. **(C)** LSR-ADC causes mitotic arrest *in vivo*. Animals bearing OVCAR3 tumor xenografts were given a single dose of PBS or LSR-ADC (1, 3, or 10 mg/kg). After 24 h, the tumors were harvested and stained with an anti-phospho-Histone H3 (Ser10) antibody to detect mitotic cells. Scale bar: 100 μm.

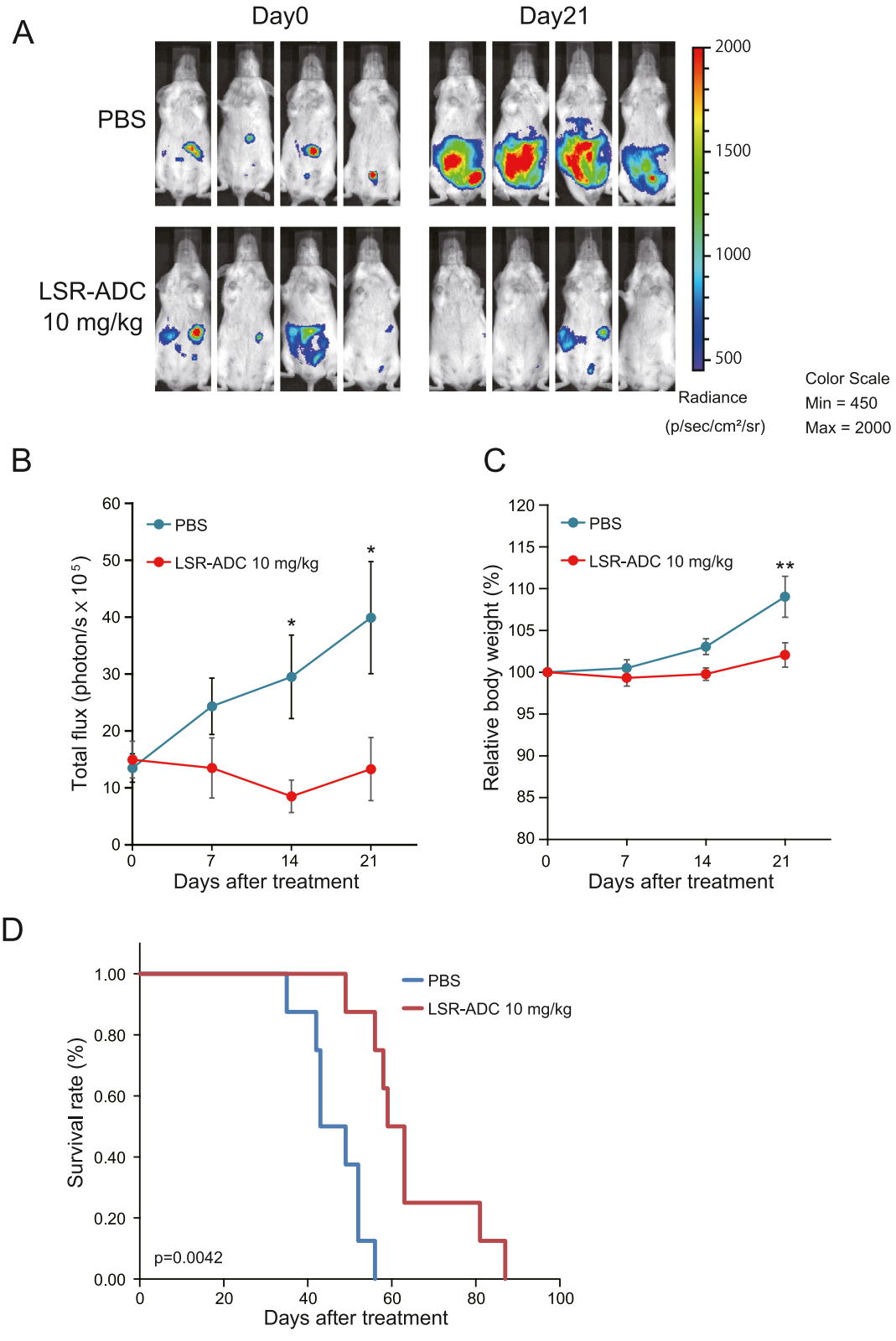

Fig. 5. Antitumor activity of LSR-ADC in ovarian cancer omental/bowel metastasis xenograft model. Bioluminescence imaging (BLI) was used to monitor the OVCAR3-Luc ovarian cancer omental/bowel metastases in the mice after intraperitoneal injection of cancer cells. The mice were randomized into PBS or 10 mg/kg LSR-ADC groups (n = 8/group) of equal average tumor burden, based on the luciferase activity at 42−49 days post-inoculation. PBS or LSR-ADC (10 mg/kg) was administered twice a week for two weeks. **(A)** Representative data of BLI detecting the OVCAR3-Luc ovarian cancer omental/bowel metastases after the intraperitoneal administration of the substrate. **(B)** Quantification of the tumor burden obtained from the OVCAR3-Luc omental/bowel metastasis study that is presented in (A). **(C)** Changes in the relative body weight. The error bars denote the SEM. **(D)** Kaplan–Meier survival analysis of the OVCAR3-Luc omental/bowel metastasis study that is presented in (A). Log-rank analysis: $p = 0.0042$ (for the LSR-ADC *versus* vehicle comparison).

shows its efficacy. The *in vitro* ADC assay revealed that OVCAR3 (LSR expression: 89,382.9/cell) and NOVC-7C (84,008.8/cell) cancer cells were sensitive to LSR-ADC, while the ES2 cells that are characterized by a low expression of LSR (2,631.9/cell), were insensitive to LSR-ADC. This suggests that certain levels of the LSR expression seem to be required for the LSR-ADC to effectively inhibit cancer cells. Secondly, more studies are needed to evaluate the *in vivo* efficacy of the developed compound in advanced EOC stages. Based on our findings on the OVCAR3-Luc omental/bowel metastasis model, we expect that the LSR-ADC may improve the survival of patients with advanced EOC, by suppressing established metastases. At present, our data have only demonstrated that the LSR-ADC directly damages the already-metastasized tumor cells in the most frequently occurring recurrence site. For example, we did not assess whether treatment with LSR-ADC can inhibit the formation or growth of metastatic lesions in the liver and the lungs; two frequently reported recurrence sites for EOC. Thirdly, our data for the LSR-ADC toxicity is limited. Although the LSR-ADC did not influence on the body weight of mice, it is desirable to conduct detailed toxicity studies before clinical application, since LSR is weakly expressed in normal human tissues such as liver [20]. We are planning to humanize anti-LSR mAb, as we have humanized another ADC without losing its efficacy [14], and then conduct detailed toxicity studies of the humanized LSR-ADC by using cynomolgus monkeys, which possess much closer antigenicity to humans than mice. Finally, the LSR expression in the platinum-resistant EOC as well as the effectiveness of LSR-ADC for such an EOC type, have not been investigated. In clinical trials, the MMAE-containing ADCs display tolerable safety profiles and clinical benefits in platinum-resistant EOC [41,42], and the herein developed LSR-ADC may have a similar effect. Our data warrant the assessment of LSR-ADC as a new therapeutic agent for patients with advanced EOC or other LSR-positive tumors.

Authors' contributions

Conception and design: Satoshi Serada and Tetsuji Naka.

Methodology development: Mizuki Kanda, Satoshi Serada.

Data acquisition: Mizuki Kanda, Satoshi Serada.

Data analysis and interpretation: Mizuki Kanda, Satoshi Serada, Kosuke Hiramatsu, Masashi Funauchi, Kengo Obata, Satoshi Nakagawa, Tomoharu Ohkawara, Okinori Murata, Minoru Fujimoto, Hiroki Sasaki, Yutaka Ueda, Tadashi Kimura, Tetsuji Naka

Manuscript writing, review, and/or revision: Mizuki Kanda, Satoshi Serada.

Administrative, technical, or material support: Satoshi Serada, Fumiko Chiwaki, Hiroki Sasaki.

Study supervision: Tetsuji Naka.

Consent for publication

Not applicable.

Data availability

All data generated and analyzed during this study are included in this published article and its supplementary information files.

Declaration of Competing Interest

S.S., M.F., and T.N. declare that a patent (US10174111B2) has been issued regarding the anti-LSR monoclonal antibody.

The authors declare the following financial interests/personal relationships which may be considered as potential competing interests:

Acknowledgments

We would like to thank K. Takahashi and C. Higuchi for their secretarial assistance, and A. Quick for her technical assistance.

Supplementary materials

Supplementary material associated with this article can be found, in the online version, at doi:10.1016/j.neo.2022.100853.

References

[1] Siegel RL, Miller KD, Jemal A. Cancer statistics, 2020. *CA Cancer J Clin* 2020;**70**(1):7–30.

[2] Japan, N.C.C., *ganjoho.jp*.

[3] Baldwin LA, et al. Ten-year relative survival for epithelial ovarian cancer. *Obstet Gynecol* 2012;**120**(3):612–18.

[4] Markman M, et al. Second-line platinum therapy in patients with ovarian cancer previously treated with cisplatin. *J Clin Oncol* 1991;**9**(3):389–93.

[5] Matsuo K, et al. Overcoming platinum resistance in ovarian carcinoma. *Expert Opin Investig Drugs* 2010;**19**(11):1339–54.

[6] Davis A, Tinker AV, Friedlander M. "Platinum resistant" ovarian cancer: what is it, who to treat and how to measure benefit? *Gynecol Oncol* 2014;**133**(3):624–31.

[7] Pujade-Lauraine E, et al. Bevacizumab combined with chemotherapy for platinum-resistant recurrent ovarian cancer: The AURELIA open-label randomized phase III trial. *J Clin Oncol* 2014;**32**(13):1302–8.

[8] Hamanishi J, et al. Safety and Antitumor Activity of Anti-PD-1 Antibody, Nivolumab, in Patients With Platinum-Resistant Ovarian Cancer. *J Clin Oncol* 2015;**33**(34):4015–22.

[9] Polakis P. Antibody Drug Conjugates for Cancer Therapy. *Pharmacol Rev* 2016;**68**(1):3–19.

[10] Birrer MJ, et al. Antibody-Drug Conjugate-Based Therapeutics: State of the Science. *J Natl Cancer Inst* 2019;**111**(6):538–49.

[11] Medicine, U.S.N.L.o., *ClinicalTrials.gov*.

[12] Lee EK, Liu JF. Antibody-drug conjugates in gynecologic malignancies. *Gynecol Oncol* 2019;**153**(3):694–702.

[13] Matsuzaki S, et al. Anti-glypican-1 antibody-drug conjugate exhibits potent preclinical antitumor activity against glypican-1 positive uterine cervical cancer. *Int J Cancer* 2018;**142**(5):1056–66.

[14] Munekage E, et al. A glypican-1-targeted antibody-drug conjugate exhibits potent tumor growth inhibition in glypican-1-positive pancreatic cancer and esophageal squamous cell carcinoma. *Neoplasia* 2021;**23**(9):939–50.

[15] Yokota K, et al. Anti-Glypican-1 Antibody-drug Conjugate as Potential Therapy Against Tumor Cells and Tumor Vasculature for Glypican-1-Positive Cholangiocarcinoma. *Mol Cancer Ther* 2021;**20**(9):1713–22.

[16] Nishigaki T, et al. Anti-glypican-1 antibody-drug conjugate is a potential therapy against pancreatic cancer. *Br J Cancer* 2020;**122**(9):1333–41.

[17] Tsujii S, et al. Glypican-1 Is a Novel Target for Stroma and Tumor Cell Dual-Targeting Antibody-Drug Conjugates in Pancreatic Cancer. *Mol Cancer Ther* 2021;**20**(12):2495–505.

[18] Nakae R, et al. CD70 antibody-drug conjugate as a potential therapeutic agent for uterine leiomyosarcoma. *Am J Obstet Gynecol* 2021;**224**(2) p. 197.e1-197.e23.

[19] Shiomi M, et al. CD70 antibody-drug conjugate: A potential novel therapeutic agent for ovarian cancer. *Cancer Sci* 2021;**112**(9):3655–68.

[20] Hiramatsu K, et al. LSR Antibody Therapy Inhibits Ovarian Epithelial Tumor Growth by Inhibiting Lipid Uptake. *Cancer Res* 2018;**78**(2):516–27.

[21] Yen FT, et al. Identification of a lipolysis-stimulated receptor that is distinct from the LDL receptor and the LDL receptor-related protein. *Biochemistry* 1994;**33**(5):1172–80.

[22] Yen FT, et al. Molecular cloning of a lipolysis-stimulated remnant receptor expressed in the liver. *J Biol Chem* 1999;**274**(19):13390–8.

[23] Takano K, et al. The Behavior and Role of Lipolysis-stimulated Lipoprotein Receptor, a Component of Tricellular Tight Junctions, in Head and Neck Squamous Cell Carcinomas. *Anticancer Res* 2016;**36**(11):5895–904.

[24] Zhang M, Ma C. LSR Promotes Cell Proliferation and Invasion in Lung Cancer. *Comput Math Methods Med* 2021;**2021**:6651907.

[25] Garcia JM, et al. Prognostic value of LISCH7 mRNA in plasma and tumor of colon cancer patients. *Clin Cancer Res* 2007;**13**(21):6351–8.

[26] Herbsleb M, et al. Increased cell motility and invasion upon knockdown of lipolysis stimulated lipoprotein receptor (LSR) in SW780 bladder cancer cells. *BMC Med Genomics* 2008;**1**:31.

[27] Reaves DK, et al. The role of lipolysis stimulated lipoprotein receptor in breast cancer and directing breast cancer cell behavior. *PLoS One* 2014;**9**(3):e91747.

[28] Sugase T, et al. Lipolysis-stimulated lipoprotein receptor overexpression is a novel predictor of poor clinical prognosis and a potential therapeutic target in gastric cancer. *Oncotarget* 2018;**9**(68):32917–28.

[29] Shimada H, et al. The roles of tricellular tight junction protein lipolysis-stimulated lipoprotein receptor in malignancy of human endometrial cancer cells. *Oncotarget* 2016;**7**(19):27735–52.

[30] Ogiwara H, et al. Targeting the Vulnerability of Glutathione Metabolism in ARID1A-Deficient Cancers. *Cancer Cell* 2019;**35**(2) p. 177-190.e8.

[31] Tanaka Y, et al. Multi-omic profiling of peritoneal metastases in gastric cancer identifies molecular subtypes and therapeutic vulnerabilities. *Nat Cancer* 2021;**2**(9):962–77.

[32] Kobayashi Y, et al. Response Predictive Markers and Synergistic Agents for Drug Repositioning of Statins in Ovarian Cancer. *Pharmaceuticals (Basel)* 2022;**15**(2).

[33] Austin CD, et al. Endocytosis and sorting of ErbB2 and the site of action of cancer therapeutics trastuzumab and geldanamycin. *Mol Biol Cell* 2004;**15**(12):5268–82.

[34] Hamilton TC, et al. Characterization of a xenograft model of human ovarian carcinoma which produces ascites and intraabdominal carcinomatosis in mice. *Cancer Res* 1984;**44**(11):5286–90.

[35] Liao JB, et al. Preservation of tumor-host immune interactions with luciferase-tagged imaging in a murine model of ovarian cancer. *J Immunother Cancer* 2015;**3**:16.

[36] Baert T, et al. The dark side of ID8-Luc2: pitfalls for luciferase tagged murine models for ovarian cancer. *J Immunother Cancer* 2015;**3**:57.

[37] Malik P, et al. Pharmacokinetic Considerations for Antibody-Drug Conjugates against Cancer. *Pharm Res* 2017;**34**(12):2579–95.

[38] Hoffmann RM, et al. Antibody structure and engineering considerations for the design and function of Antibody Drug Conjugates (ADCs). *Oncoimmunology* 2018;**7**(3):e1395127.

[39] Goldmacher VS, Kovtun YV. Antibody-drug conjugates: using monoclonal antibodies for delivery of cytotoxic payloads to cancer cells. *Ther Deliv* 2011;**2**(3):397–416.

[40] Okajima D, et al. Datopotamab Deruxtecan, a Novel TROP2-directed Antibody-drug Conjugate, Demonstrates Potent Antitumor Activity by Efficient Drug Delivery to Tumor Cells. *Mol Cancer Ther* 2021;**20**(12):2329–40.

[41] Banerjee S, et al. Anti-NaPi2b antibody-drug conjugate lifastuzumab vedotin (DNIB0600A) compared with pegylated liposomal doxorubicin in patients with platinum-resistant ovarian cancer in a randomized, open-label, phase II study. *Ann Oncol* 2018;**29**(4):917–23.

[42] Liu J, et al. An open-label phase I dose-escalation study of the safety and pharmacokinetics of DMUC4064A in patients with platinum-resistant ovarian cancer. *Gynecol Oncol* 2021;**163**(3):473–80.